

# Modified Viterbi-Based Local-Multipath Doppler Difference Estimation in Over-the-Horizon Radar

Vaishali S. Amin<sup>†</sup>, Yimin D. Zhang<sup>†</sup>, and Braham Himed<sup>‡</sup>

<sup>†</sup> Department of Electrical and Computer Engineering, Temple University, Philadelphia, PA, 19122, USA

<sup>‡</sup> Distributed RF Sensing Branch, Air Force Research Laboratory, AFRL/RYSM, Dayton, OH, 45433, USA

**Abstract**—In sky-wave over-the-horizon radar, local multipath returns from a maneuvering target, generated as a result of reflections from ionosphere and earth surfaces, generally yield three distinct components with highly time-varying and closely separated Doppler frequencies. The difference between these Doppler signatures provides important information on target velocity in the elevation direction and enables high-resolution target altitude estimation. However, it is often a challenging task to accurately estimate this Doppler difference due to the proximity of the Doppler components. In this paper, we develop a low-complexity modified Viterbi-based approach to provide improved Doppler difference estimation in impaired observing conditions. Simulation results verify the effectiveness of the proposed method.

**Index Terms**—Doppler frequency, over-the-horizon radar, target tracking, time-frequency analysis, Viterbi-based estimation.

## I. INTRODUCTION

By utilizing reflections and refractions from the ionospheric layers and the earth surface, a sky-wave over-the-horizon radar (OTHR) performs wide-area surveillance to detect targets which are located well beyond the coverage of conventional line-of-sight radars [1]. In OTHR, prevalent ionospheric conditions limit the signal to be narrowband, which, in turn, adversely affects the achieved range resolution [2]. The range resolution of an OTHR system is usually around 10 kilometers [3]. While this accuracy is acceptable when considering the horizontal positions of targets located at thousands of kilometers away, it makes the direct estimation of target altitude impractical, as the altitude of a typical aircraft is comparable to the available range resolution. Target altitude estimation with a higher resolution is important for target position tracking as well as for its classification [4].

In practice, reflections of radar signals from ionospheric layers and the earth surface generate local-multipath observations. Doppler frequencies associated with these multipath signals contain important information about target parameters. In particular, the difference between these Doppler signatures carries important information regarding the target elevation velocity, which is crucial for accurate and high-resolution target altitude estimation and tracking [5, 6].

However, this Doppler difference between local-multipath signals is extremely small, making its accurate estimation a challenging task. Time-frequency (TF) techniques [7, 8] facilitate visualization and analysis of these Doppler signatures. In the past two decades, various techniques devised based on the local-multipath model have attempted to resolve these Doppler signatures to enable high-resolution target parameter estimation in OTHR [4, 6, 9–13]. However, these techniques suffer from either a high computational complexity, requirement of exhaustive parametric analysis, or insufficient resolution. The close proximity of these highly time-varying and non-linear Doppler components, inherent interference, and low signal-to-noise ratio (SNR) adversely affect the performance of these methods.

An important approach attempts to stationarize (demodulate) the local-multipath signals with its nominal Doppler frequency [6, 11]. However, accurate estimation of the nominal Doppler frequency is highly time consuming, and any inaccurate nominal Doppler frequency estimation will result in erroneous Doppler difference estimation. Recently, by utilizing prior information of these Doppler characteristics, a self demodulation-based low-complexity approach was developed to eliminate the need for nominal Doppler component estimation [14], in which a squared magnitude operation guarantees perfect signal stationarization and generates four symmetric components located around the direct-current (DC) component. Then, the short-time Fourier transform (STFT)-based approach is utilized to obtain the targeted Doppler frequency difference in [14]. However, due to the low frequency resolution of STFT, this approach does not provide satisfactory accuracy, particularly when multiple Doppler difference components are not well separated.

This self-demodulation concept is extended in [15], where Doppler difference estimation is formulated as a group-sparse reconstruction problem to take advantage of the relationship between these Doppler signatures. While this method provides robust Doppler difference estimation, Bayesian compressive sensing-based optimization approaches [16, 17] are generally computationally extensive. Besides, the performance of parametric approaches seriously deteriorates in the case of model mismatch.

Recently developed non-parametric TF methods [18–21] provide robust instantaneous frequency (IF) estimation of sparse non-linear frequency modulated (FM) signals. However, these methods either require cumbersome manual tuning of the parameters, are computationally expensive, suffer from

---

The work of V. S. Amin and Y. D. Zhang is supported in part by a subcontract with Matrix Research, Inc. for research sponsored by the Air Force Research Laboratory under contract FA8650-14-D-1722. The work of Y. D. Zhang is also supported in part by a contract with Altamira Technologies Corp. for research sponsored by the Air Force Research Laboratory under contract FA8650-18-C-1055.

frequency quantization errors, or rely on the accuracy of the underlying TF representations (TFRs). Besides, impaired observing conditions and proximity of the Doppler signatures in OTHR may adversely affect the performance of these methods.

Generalized Viterbi-based [22] IF estimation is considered in various papers [12, 23–25], in which recursive implementation of Viterbi-based IF estimation greatly reduces the search space by selecting the partial best paths. In addition, Viterbi-based IF estimation methods are shown to be effective in impaired observing environments. Implementation of Viterbi-based OTHR Doppler signatures estimation is considered in [12], where separate estimation, stationarization and removal of all Doppler signatures are required, and Doppler difference is indirectly obtained by computing the difference between the estimated signatures. Due to the proximity of these Doppler components, these steps are repeated a few times, which greatly increase complexity and yet give inaccurate estimation of the nominal Doppler component and Doppler difference.

We observe that only the difference Doppler component needs to be estimated for acquiring target elevation velocity. Therefore, when estimating Doppler difference is of interest, estimation of the nominal frequency component is not required. In this scenario, implementation of a modified Viterbi-based technique on the squared magnitude of the received signal [14, 15] would provide much simpler, yet more accurate and robust, Doppler difference estimation. Our proposed modified Viterbi-based Doppler difference estimation algorithm is founded on this important observation. By carefully drafting the conditions of the penalty function based on the Doppler characteristics in OTHR, the proposed technique overcomes the limitation of the existing Doppler difference approaches [12, 14, 15] and provides robust, accurate and high-resolution Doppler difference estimation with much lower computational complexity than the methods reported in [12, 15]. Simulation results are provided to validate the superiority of the proposed method over existing techniques.

*Notations.* An uppercase bold letter defines a matrix.  $(\cdot)^*$  represents the complex conjugation operation. In addition, we use  $j$  to denote the unit imaginary number.

## II. SIGNAL MODEL

Fig. 1 shows the multipath propagation geometry for the considered pseudo-monostatic OTHR system, in which the signal propagates through a stable E-layer of the ionosphere. For simplicity of the mathematical analysis, a flat-earth model is considered. In Fig. 1,  $R(t)$  and  $h(t)$  denote the time-varying target ground range and its altitude, respectively, and  $H$  is the height of the ionosphere, which is assumed to be constant over the processing interval and is known from periodic ionosonde measurements. In Fig. 1, the objects and paths below the ionosphere layer depict the physical system, whereas the mirrored images are provided above the ionosphere layer for visualization purposes only.

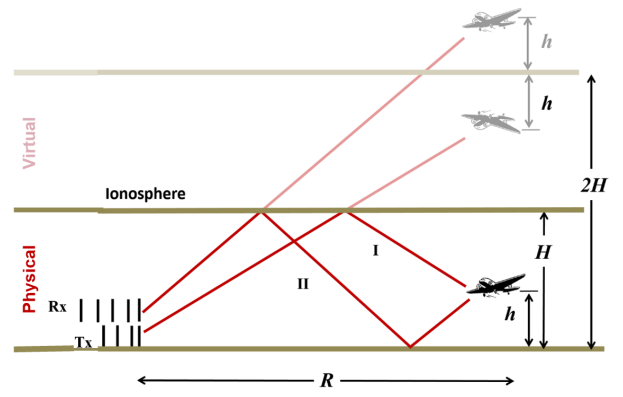


Fig. 1: Flat-earth local-multipath propagation model with its mirrored images.

Based on Fig. 1, the slant ranges associated with multipaths I and II are, respectively, computed as

$$\begin{aligned} l_1(t) &= (R^2(t) + (2H - h(t))^2)^{1/2}, \\ l_2(t) &= (R^2(t) + (2H + h(t))^2)^{1/2}. \end{aligned} \quad (1)$$

In practice,  $h(t) \ll H \ll R(t)$  typically holds. In this case, the slant ranges are approximated using the Taylor series expansion as

$$l_1(t) \approx R(t) + \frac{2H^2 - 2Hh(t)}{R(t)}, \quad l_2(t) \approx R(t) + \frac{2H^2 + 2Hh(t)}{R(t)}, \quad (2)$$

and their derivatives with respect to time are obtained as

$$\begin{aligned} \frac{dl_1(t)}{dt} &\approx v_R(t) - \frac{2H^2}{R^2(t)}v_R(t) - \frac{2H}{R(t)}v_h(t), \\ \frac{dl_2(t)}{dt} &\approx v_R(t) - \frac{2H^2}{R^2(t)}v_R(t) + \frac{2H}{R(t)}v_h(t), \end{aligned} \quad (3)$$

where  $v_R(t) = dR(t)/dt$  and  $v_h(t) = dh(t)/dt$  represent the target velocities in range and altitude directions, respectively.

Denote  $f_c$  as the carrier frequency,  $c$  as the speed of the electromagnetic wave propagation, and  $J(t) = 1 - 2H^2/R^2(t)$ . Let  $f_{11}(t)$ ,  $f_{22}(t)$ ,  $f_{12}(t)$ , and  $f_{21}(t)$ , respectively, represent the Doppler frequencies associated with multipaths  $I_t$ - $I_r$  (i.e., the signal is transmitted through path I and received through path I),  $II_t$ - $II_r$ ,  $I_t$ - $II_r$ , and  $II_t$ - $I_r$ , and are given as

$$\begin{aligned} f_{11}(t) &= -\frac{2f_c}{c} \frac{dl_1(t)}{dt} \approx -\frac{2f_c}{c} J(t)v_R(t) + \frac{4f_c H}{R(t)c} v_h(t), \\ f_{22}(t) &= -\frac{2f_c}{c} \frac{dl_2(t)}{dt} \approx -\frac{2f_c}{c} J(t)v_R(t) - \frac{4f_c H}{R(t)c} v_h(t), \\ f_{12}(t) &= f_{21}(t) = -\frac{f_c}{c} \frac{dl_1(t) + dl_2(t)}{dt} \approx -\frac{2f_c}{c} J(t)v_R(t). \end{aligned} \quad (4)$$

By defining the nominal Doppler component as

$$f_N(t) = -\frac{2f_c}{c} J(t)v_R(t), \quad (5)$$

and the difference Doppler component as

$$f_D(t) = \frac{4f_c H v_h(t)}{R(t)c}, \quad (6)$$

(4) can be simplified to

$$\begin{aligned} f_{11}(t) &= f_N(t) + f_D(t), \\ f_{22}(t) &= f_N(t) - f_D(t), \\ f_{12}(t) &= f_{21}(t) = f_N(t). \end{aligned} \quad (7)$$

Note in (4) and (7) that the Doppler signatures of the first two paths, i.e.,  $f_{11}(t)$  and  $f_{22}(t)$ , are symmetric around the frequencies associated with the third and fourth multipath,  $f_{12}(t) = f_{21}(t)$ . The associated phase laws are given by

$$\begin{aligned} \phi_1(t) &= -2\pi \int_0^t (f_N(t) + f_D(t))dt = \phi_N(t) - \phi_D(t), \\ \phi_2(t) &= -2\pi \int_0^t (f_N(t) - f_D(t))dt = \phi_N(t) + \phi_D(t), \\ \phi_3(t) &= \phi_4(t) = -2\pi \int_0^t f_N(t)dt = \phi_N(t), \end{aligned} \quad (8)$$

where  $\phi_N(t) = 4\pi f_c J(t)R(t)/c$  and  $\phi_D(t) = 8\pi f_c Hh(t)/(R(t)c)$ . Note that in the derivations of the phase laws,  $R(t)$  is treated as a constant due to the insignificant effect of its change over the processing interval.

Denote the received signal obtained after matched filtering and beamforming at the receiver as

$$x(t) = r(t) + \eta(t), \quad (9)$$

for  $t = 1, \dots, T$ , where  $T$  is the total number of time samples,  $\eta(t)$  is the zero-mean complex white Gaussian noise, and  $r(t)$  defines the noise-free target return, expressed as

$$r(t) = \sum_{n=1}^3 a_n \exp(j\phi_n(t)), \quad (10)$$

where  $a_n$  denotes the magnitude of the  $n$ th path. Note that, because  $\phi_3(t) = \phi_4(t)$ , these two components are combined and  $a_3$  accounts for the contribution from both components.

### III. PROPOSED DOPPLER DIFFERENCE ESTIMATION

From (5)–(7), it is clear that the nominal Doppler component,  $f_N(t)$ , is shared by all three paths and provides information on the target horizontal velocity  $v_R$ , whereas the difference Doppler component,  $f_D(t)$ , carries information regarding the target elevation velocity  $v_h(t)$ . Generally,  $v_h(t) \ll v_R(t)$ , and thus  $f_D(t)$  is much smaller compared to  $f_N(t)$ . As such, accurate estimation of  $f_D(t)$  is challenging when the nominal Doppler frequency  $f_N(t)$  associated with a maneuvering target is highly non-linear. The primary interest of this work is to obtain accurate and high-resolution Doppler difference estimation, which plays a vital role in high-accuracy target altitude estimation, with a low complexity.

In this section, we describe the proposed method, which is performed in two stages: 1) stationarization and nominal Doppler component removal and 2) difference Doppler signature estimation using modified Viterbi-based IF estimation.

#### A. Stationarization and Nominal Component Removal

To remove the nominal Doppler component without the need of performing its accurate estimation, we multiply the

received multi-component signal with its complex conjugate [14, 15], i.e.,

$$|x(t)|^2 = |r(t)|^2 + |\eta(t)|^2 + \epsilon(t) = |r(t)|^2 + \Lambda(t), \quad (11)$$

where  $\epsilon(t)$  represents the cross-terms between  $r(t)$  and  $\eta(t)$ , and  $\Lambda(t)$  represents the combined effect of the noise and cross-terms and will be referred to as the noise term, without loss of generality.

In (11), the squared magnitude of the noise-free target return,  $r(t)$ , is expressed as

$$\begin{aligned} |r(t)|^2 &= (|a_1|^2 + |a_2|^2 + |a_3|^2) \\ &\quad + (a_1 a_3^* + a_2^* a_3) \exp(j\phi_D(t)) \\ &\quad + (a_1^* a_3 + a_2 a_3^*) \exp(-j\phi_D(t)) \\ &\quad + a_1 a_2^* \exp(j2\phi_D(t)) + a_1^* a_2 \exp(-j2\phi_D(t)). \end{aligned} \quad (12)$$

After the self-demodulation operation of (12), the nominal Doppler component is removed and only the phase term related to the difference Doppler component,  $\phi_D(t)$ , is preserved. Although the demodulation operation in (12) generates four localized components which are symmetrically located around the DC component, we only need to estimate  $\phi_D(t)$  corresponding to the fundamental frequency component in order to obtain the elevation velocity of the maneuvering target. Thus, this technique provides much simpler, yet more accurate, Doppler difference estimation as compared to [6, 11].

#### B. Modified Viterbi-based Doppler Difference Estimation

We begin with the TF analysis of the demodulated Doppler difference signatures  $|x(t)|^2$  from (11). Due to the symmetry of these signatures, consideration of only the positive half of the TFR is required, thereby reducing the complexity of the Viterbi-based IF estimation. Let an  $M \times T$  TF matrix  $\mathbf{Y} = \{(t_i, f_j) | i \in [1, T], j \in [1, M]\}$  represent the selected positive half portion of the TFR of  $|x(t)|^2$ , where  $M$  and  $T$ , respectively, define the total number of frequency bins and the total number of time samples,  $(t_i, f_j)$  denotes a TF point, and  $i$  and  $j$ , respectively, represent the time and frequency indices.

As the DC component in the stationarized signal has a high value but does not provide useful information related to the Doppler difference frequency, it is removed through low-pass filtering.

Let set  $\mathcal{S}$  comprise all the paths,  $S(t)$ , between the time instances  $t_1$  and  $t_T$  for the considered time interval  $t \in [t_1, t_T]$ , and  $p(S(t); t_1, t_T)$  denote the penalty function of the path joining  $t_1$  and  $t_T$ , along the line  $S(t)$ . Then, the Doppler difference frequency for each time instant,  $t$ , is obtained by selecting the path that minimizes the penalty function, as

$$\hat{f}(t) = \arg \min_{S(t) \in \mathcal{S}} p(S(t); t_1, t_T). \quad (13)$$

The penalty function is designed based on the following criteria:

- The IF path should pass through high energy points. In order to implement this constraint, first we sort all TF points at instant  $t$  in the descending order of their amplitude levels, i.e.,

$$y(t, f_1(t)) \geq y(t, f_2(t)) \geq \dots \geq y(t, f_M(t)), \quad (14)$$

where  $y(t, f_m(t))$ ,  $m \in [1, M]$ , is the amplitude of TF point  $(t, f_m(t))$ , and  $f_m(t)$  indicates the index of the frequency corresponding to the  $m$ th highest amplitude TF point at time  $t$ . Then, the penalty function

$$g_1(y(t, f_m(t))) = m - 1 \quad (15)$$

assigns a penalty of 0 point to the highest amplitude TF point and the lowest amplitude TF point is assigned the penalty of  $M - 1$  points.

- For an OTHR target, the IF is a slowly time-varying function. Therefore, the second criterion is designed to discourage swift changes in the IF estimates of two consecutive time instances by assigning a high penalty to such sudden jumps. The associated penalty function is defined as

$$g_2(a(t), b(t+1)) = \begin{cases} 0, & q \leq \xi_1, \\ c_1(q - \xi_1), & \xi_1 < q \leq \xi_2, \\ c_2(q - \xi_1), & \xi_2 < q, \end{cases} \quad (16)$$

where  $a(t)$  and  $b(t+1)$  are the indices of the frequencies in two consecutive time instances  $t$  and  $t+1$ , respectively, and  $q = |a(t) - b(t+1)|$  represents their distance as an integer. Thresholds  $\xi_1$  and  $\xi_2$ , where  $\xi_2 > \xi_1$ , are defined in terms of the number of frequency bins. The penalties  $c_1$  and  $c_2$  with  $c_2 > c_1$  are also defined as integer values. These relationships and the conditions of penalty function  $g_2(\cdot)$  ensure that a moderate penalty is assigned to insignificant jumps, whereas high abrupt jumps are penalized with higher values. The selection of the values of  $\xi_1$ ,  $\xi_2$ ,  $c_1$ , and  $c_2$  depends on the characteristics of the underlying signal. For highly non-linear signals,  $\xi_1$  and  $\xi_2$  should be assigned higher values, whereas lower values should be assigned to  $c_1$  and  $c_2$ , and vice-versa.

Based on (15) and (16), the overall penalty function is given as

$$p(S(t); t_1, t_T) = \sum_{t=t_1}^{t_T} g_1(y(t, S(t))) + \sum_{t=t_1}^{t_T-1} g_2(S(t), S(t+1)). \quad (17)$$

The optimization problem in (13) is recursively solved as an instance of generalized Viterbi algorithm [22] by estimating the Doppler difference frequency at a given time instant using partial best paths from the previous time instant [23, 24] as follows:

**Step 1.** Denote  $\pi_i(t; f_j)$ ,  $t \in [t_1, t_i]$ , for  $j \in [1, M]$  as the optimal paths (also known as *partial best paths*) connecting instant  $t_1$  and all the points of instant  $t_i$ , and are obtained as

$$\pi_i(t; f_j) = \arg \min_{S(t) \in \mathcal{S}_{ij}} p(S(t); t_1, (t_i, f_j)), \quad j \in [1, M], \quad (18)$$

where set  $\mathcal{S}_{ij}$  comprises all the paths between instant  $t_1$  and TF point  $(t_i, f_j)$ , whereas  $p(S(t); t_1, (t_i, f_j))$  denotes the corresponding penalty function. Then, the Doppler frequency for  $t \in [t_1, t_i]$  can be obtained as

$$\hat{f}_i(t) = \arg \min_{\pi_i(t; f_j), j \in [1, M]} p(\pi_i(t; f_j); t_1, (t_i, f_j)). \quad (19)$$

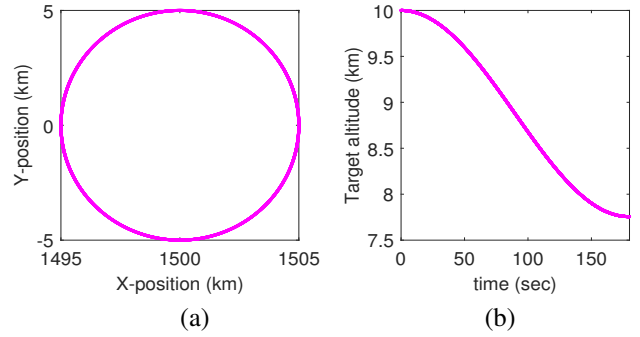


Fig. 2: Target trajectory: (a) Horizontal positions; (b) Altitude.

TABLE I. KEY PARAMETERS

Parameter	Notation	Value
Initial range of target	$R(0)$	1,500 km
Initial height of target	$h(0)$	10 km
Maximum range direction velocity	$v_{R,\max}$	175 m/s
Maximum elevation velocity	$v_{h,\max}$	19.68 m/s
Height of ionosphere	$H$	160 km
Carrier frequency	$f_c$	16 MHz
Pulse repetition frequency	$f_w$	40 Hz

**Step 2.** The partial best paths at the next instant  $t_{i+1}$  can be represented as the concatenation of (18) with the TF points at the new instant as

$$\pi_{i+1}(t; f_j) = [\pi_i(t; \hat{f}_i), (t_{i+1}, f_j)], \quad j \in [1, M], \quad (20)$$

where the frequency index  $\hat{l}$  of the optimal path  $\pi_i(t; f_j)$  corresponding to the previous instant  $t_i$  is obtained as

$$\hat{l} = \arg \min_{l \in [1, M]} [p(\pi_i(t; f_l); t_1, (t_i, f_l)) + g_1(y(t_{i+1}, f_j)) + g_2(f_l, f_j)]. \quad (21)$$

Note that the function  $g_1(y(t_{i+1}, f_j))$  is a constant for the considered partial best path. Step 2 is repeated for each  $f_j$ ,  $j \in [1, M]$ . Steps 1 and 2 are repeated for all the time instances, i.e.,  $t_i = t_2, \dots, t_{T-1}$ .

In this work, we use spectrogram as the TFR  $\mathbf{Y}$ . However, other TFRs [19–21, 26, 27] can also be used in lieu of spectrogram for further improvement and resolution enhancement, generally at the cost of higher computational complexity.

#### IV. SIMULATION RESULTS

In order to demonstrate the effectiveness of the proposed method, we consider the scenario of a maneuvering aircraft which makes a  $360^\circ$  circular turn of a 10 km diameter in a time period of  $T_0 = 179.5$  seconds while it descends by 2.25 km [14, 15]. The aircraft maintains a constant horizontal velocity of 175 m/s, while its elevation velocity changes sinusoidally. Fig. 2 illustrates the aircraft trajectory. The other key simulation parameters are listed in Table I.

The elevation velocity of the aircraft is expressed as

$$v_h(t) = -v_{h,\max} \sin\left(\frac{\pi t}{T_0}\right), \quad (22)$$

and the corresponding altitude of the aircraft is obtained as

$$h(t) = h(0) - \frac{v_{h,\max} T_0}{\pi} \left[ 1 - \cos\left(\frac{\pi t}{T_0}\right) \right]. \quad (23)$$

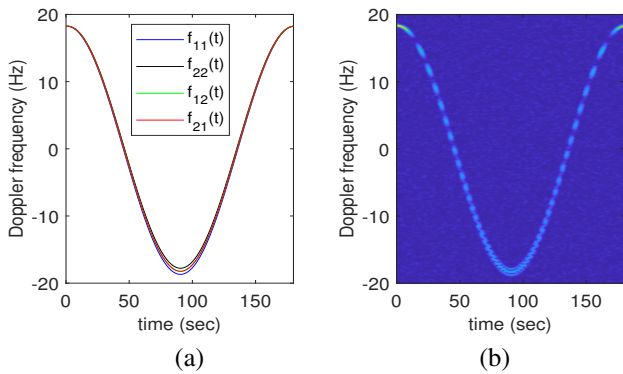


Fig. 3: Multipath Doppler frequencies: (a) True signatures corresponding to  $r(t)$ ; (b) Spectrogram of noisy signal  $x(t)$ .

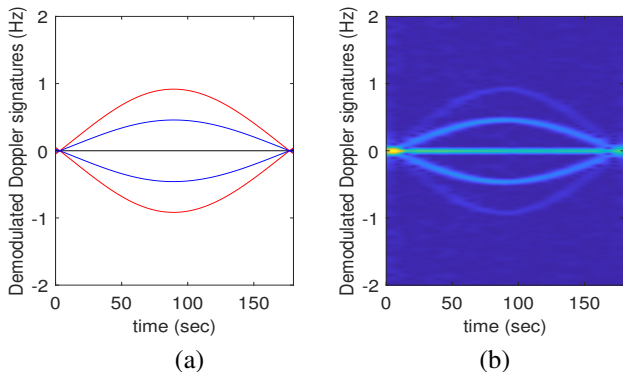


Fig. 4: Demodulated Doppler signatures: (a) True signatures; (b) Spectrogram.

All local-multipath returns are assumed to fall in the same range cell. The effective input SNR after match filtering and beamforming at the receiver is assumed to be 0 dB. We consider a clutter-free scenario under the assumption that the clutter is located in the low-frequency regions and can be filtered out using, e.g., auto-regressive pre-whitening techniques [4, 28].

Four multipath-generated true Doppler frequency signatures corresponding to  $r(t)$  are depicted in Fig. 3(a), whereas Fig. 3(b) shows the corresponding spectrogram of the noisy received signal  $x(t)$ . Using (5) and (6), the peak values of  $f_N(t)$  and  $f_D(t)$  are obtained as 18.66 Hz and 0.4478 Hz, respectively. As these Doppler signatures are highly non-linear and  $f_D(t) \ll f_N(t)$ , it is extremely difficult to directly resolve these Doppler signatures, as can also be verified in Fig. 3.

Figs. 4(a) and 4(b) show the true demodulated Doppler signatures corresponding to  $|r(t)|^2$  and the spectrogram corresponding to the noisy signal  $|x(t)|^2$ , respectively. While the spectrogram depicted in Fig. 4(b) shows the general trend of the time-varying Doppler frequency difference, it suffers from poor frequency resolution and is highly affected by noise and harmonic interference, especially when the Doppler frequency difference is small.

The comparison between the estimated Doppler difference results obtained using different approaches is provided in Fig. 5. Figs. 5(a), 5(c), and 5(e) show the TFRs of the estimated

Doppler difference obtained using the spectrogram, the group-sparsity based method [15], and the proposed Viterbi-based estimation method, respectively. The corresponding IFs are plotted in Figs. 5(b), 5(d) and 5(f), respectively. The true IFs are also provided for comparison. Note that, due to the symmetry of the demodulated Doppler difference signatures around the DC component in Fig. 4, we only need to estimate the difference Doppler component related to the fundamental frequency. By substituting (22) into (6), it is inferred that, in the underlying example, the difference Doppler component  $f_D(t)$  varies sinusoidally with time, as can be confirmed in Fig. 5.

The spectrogram in Fig. 5(a) is obtained by fusing the demodulated Doppler difference signatures [14]. The corresponding Doppler difference in Fig. 5(b) is obtained using peak detection. As clearly visible in Figs. 5(a) and 5(b), the spectrogram exhibits cross-terms, suffers from low frequency resolution, and fails to provide accurate estimation when the Doppler difference is small. The group-sparsity based approach, depicted in Figs. 5(c) and 5(d), performs better than the spectrogram in terms of robustness to noise, and provides high-resolution Doppler difference estimation. However, the estimated Doppler differences still deviate from the true ones in many cases. As evident from Figs. 5(e) and 5(f), the proposed approach provides superior Doppler difference estimation results with higher accuracy, high resolution and effective cross-term and noise suppression. The values of thresholds  $\xi_1$  and  $\xi_2$ , and penalties  $c_1$  and  $c_2$  used in (16) are, respectively, taken as 3, 10, 30 and 100. The average root mean square error (RMSE) values obtained from 50 independent trials of the estimated Doppler difference using the spectrogram, the group-sparsity-based method [15], and the proposed technique are 0.0281 Hz, 0.0234 Hz, and 0.0067 Hz, respectively. As such, the superiority of the proposed method is clearly verified.

## V. CONCLUSION

In this paper, we proposed a modified Viterbi-based approach for accurate and robust estimation of the difference Doppler component corresponding to local multipath target returns in OTHR systems. By effectively crafting the conditions of the modified Viterbi algorithm based on the Doppler characteristics of the multipath signals, the proposed approach provides better results with much lower computational complexity and high-resolution compared to recently developed Doppler difference estimation methods. Simulation results validated the effectiveness of the proposed method.

## REFERENCES

- [1] A. A. Kolosov, *Over-the-Horizon Radar*. Artech House, 1987.
- [2] J. M. Headrick and S. J. Anderson, "HF over-the-horizon radar," Chapter 20 in M. Skolnik (ed.), *Radar Handbook, 3rd Ed.* McGraw-Hill, 2008.
- [3] G. A. Fabrizio (ed.), *High Frequency Over-the-Horizon Radar: Fundamental Principles, Signal Processing, and Practical Applications*. McGraw-Hill, 2013.
- [4] Y. Zhang, M. G. Amin, and G. J. Frazer, "High-resolution time-frequency distributions for manoeuvring target detection

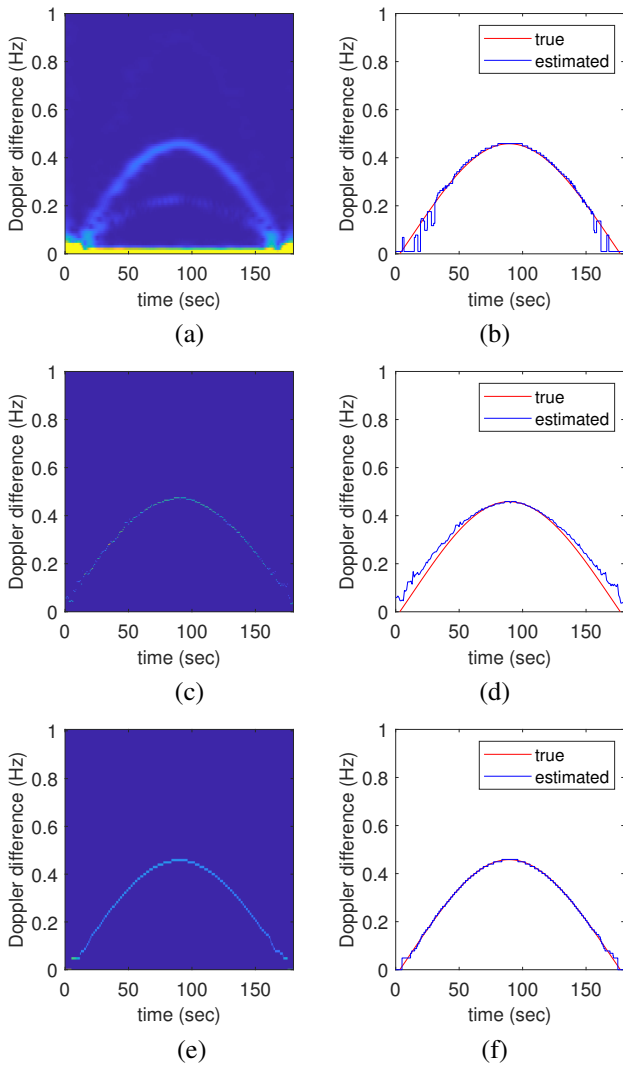


Fig. 5: Difference Doppler estimation: (a) Spectrogram; (b) Peak detection result from (a); (c) TFR from group sparsity-based method [15]; (d) Peak detection result from (c); (e) TFR from the proposed method; (f) Estimated IF from (e).

in over-the-horizon radars,” in *Proc. IEEE Radar Sonar Navig.*, vol. 150, no. 4, Nov. 2003, pp. 299–304.

- [5] R. H. Anderson, S. Kraut, and J. L. Krolik, “Robust altitude estimation for over-the-horizon radar using a state-space multipath fading model,” *IEEE Trans. Aerospace Electron. Syst.*, vol. 39, no. 1, pp. 192–201, Jan. 2003.
- [6] Y. D. Zhang, J. J. Zhang, M. G. Amin, and B. Himed, “Instantaneous altitude estimation of maneuvering targets in over-the-horizon radar exploiting multipath Doppler signatures,” *EURASIP J. Adv. Signal Process.*, vol. 2013, no. 2013:100, pp. 1–13, May 2013.
- [7] L. Cohen, *Time-Frequency Analysis*. Prentical Hall, 1995.
- [8] V. Chen and H. Ling, *Time-Frequency Transforms for Radar Imaging and Signal Analysis*. Aetech House, 2002.
- [9] C. Ioana, M. G. Amin, Y. D. Zhang, and F. Ahmad, “Characterization of Doppler effects in the context of over-the-horizon radar,” in *Proc. IEEE Radar Conf.*, Washington, D.C., May 2010, pp. 506–510.
- [10] Y. D. Zhang, M. G. Amin, and B. Himed, “Altitude estimation of maneuvering targets in MIMO over-the-horizon radar,” in *Proc. IEEE Sensor Array Multichannel Signal Process. (SAM)*

*Workshop*, Hoboken, NJ, June 2012, pp. 257–260.

- [11] C. Ioana, Y. D. Zhang, M. G. Amin, F. Ahmad, G. Frazer, and B. Himed, “Time-frequency characterization of micro-multipath signals in over-the-horizon radar,” in *Proc. IEEE Radar Conf.*, Atlanta, GA, May 2012, pp. 671–675.
- [12] I. Djurovic, S. Djukanovic, M. G. Amin, Y. D. Zhang, and B. Himed, “High-resolution time-frequency representations based on the local polynomial Fourier transform for over-the-horizon radars,” in *Proc. SPIE Defense Security Sensing Conf.*, vol. 8361, Baltimore, MD, May 2012.
- [13] I. Djurovic and Y. D. Zhang, “Accurate parameter estimation of over-the-horizon radar signals using RANSAC and MUSIC algorithms,” *Progress In Electromagnetics Research M*, vol. 67, pp. 85–93, April 2018.
- [14] Y. D. Zhang and B. Himed, “Multipath Doppler difference estimation in over-the-horizon radar,” in *Proc. IEEE Radar Conf.*, Oklahoma City, OK, April 2018, pp. 0693–0697.
- [15] V. S. Amin, Y. D. Zhang, and B. Himed, “Group sparsity-based local multipath Doppler difference estimation in over-the-horizon radar,” in *Proc. IEEE Int. Radar Conf.*, Washington, DC, April 2020, pp. 436–441.
- [16] Z. Zhang and B. D. Rao, “Extension of SBL algorithms for the recovery of block sparse signals with intrablock correlation,” *IEEE Trans. Signal Process.*, vol. 61, no. 8, pp. 2009–2015, April 2013.
- [17] S. Ji, D. Dunson, and L. Carin, “Multitask compressive sensing,” *IEEE Trans. Signal Proc.*, vol. 57, no. 1, pp. 92–106, Jan. 2009.
- [18] V. S. Amin, Y. D. Zhang, and B. Himed, “Sparsity-based time-frequency representation of FM signals with burst missing samples,” *Signal Process.*, vol. 155, pp. 25–43, Feb. 2019.
- [19] V. S. Amin, Y. D. Zhang, and B. Himed, “Improved instantaneous frequency estimation of multi-component FM signals,” in *Proc. IEEE Radar Conf.*, Boston, MA, April 2019.
- [20] S. Zhang and Y. D. Zhang, “Robust time-frequency analysis of multiple FM signals with burst missing samples,” *IEEE Signal Process. Lett.*, vol. 26, no. 8, pp. 1172–1176, June 2019.
- [21] V. S. Amin, Y. D. Zhang, and B. Himed, “Sequential time-frequency signature estimation of multi-component FM signals,” in *Proc. Asilomar Conf. Signals Syst. Comp.*, Pacific Grove, CA, Nov. 2019, pp. 1901–1905.
- [22] G. D. Forney, “The Viterbi algorithm,” in *Proc. IEEE*, vol. 61, no. 3, pp. 268–278, March 1973.
- [23] I. Djurovic and L. J. Stankovic, “An algorithm for the Wigner distribution based instantaneous frequency estimation in a high noise environment,” *IEEE Signal Process.*, vol. 84, no. 3, pp. 631–643, March 2004.
- [24] N. A. Khan, M. Mohammadi, and I. Djurovic, “A modified Viterbi algorithm-based IF estimation algorithm for adaptive directional time-frequency distributions,” *Circuits Syst. Signal Process.*, vol. 38, pp. 2227–2244, May 2019.
- [25] N. A. Khan, M. Mohammadi, and I. Stankovic, “Sparse reconstruction based on iterative TF domain filtering and Viterbi based IF estimation algorithm,” *Signal Process.*, vol. 166, pp. 1–12, Jan. 2020.
- [26] V. S. Amin, Y. D. Zhang, and B. Himed, “Improved IF estimation of multi-component FM Signals through iterative adaptive missing data recovery,” in *Proc. IEEE Radar Conf.*, Florence, Italy, Sept. 2020.
- [27] V. S. Amin, Y. D. Zhang, and B. Himed, “Improved time-frequency representation of multi-component FM Signals with compressed observations,” in *Proc. Asilomar Conf. Signals Syst. Comp.*, Pacific Grove, CA, Nov. 2020.
- [28] T. J. Nohara and S. Haykin, “AR-based growler detection in sea clutter,” *IEEE Trans. Signal Process.*, vol. 41, no. 3, pp. 1259–1271, March 1993.